Title	Resonance Raman scattering in bulk 2H-MX2 (M=Mo, W; X=S, Se) and monolayer MoS2
Author(s)	Fan, JH; Gao, P; Zhang, AM; Zhu, B; Zeng, H; Cui, X; He, R; Zhang, QM
Citation	Journal of Applied Physics, 2014, v. 115 n. 5, p. 053527:1-053527:7
Issued Date	2014
URL	http://hdl.handle.net/10722/197632
Rights	Journal of Applied Physics. Copyright © American Institute of Physics.

Resonance Raman scattering in bulk 2H-MX2 (M=Mo, W; X=S, Se) and monolayer MoS2

Jia-He Fan, Po Gao, An-Min Zhang, Bai-Ren Zhu, Hua-Ling Zeng, Xiao-Dong Cui, Rui He, and Qing-Ming Zhang

---

Articles you may be interested in

Facile synthesis of MoS2 and MoxW1-xS2 triangular monolayers
APL Mat. **2**, 092514 (2014); 10.1063/1.4895469

Mechanical and thermal properties of h-MX2 (M=Cr, Mo, W; X=O, S, Se, Te) monolayers: A comparative study
Appl. Phys. Lett. **104**, 203110 (2014); 10.1063/1.4879543

Ballistic performance comparison of monolayer transition metal dichalcogenide MX2 (M = Mo, W; X = S, Se, Te) metal-oxide-semiconductor field effect transistors
J. Appl. Phys. **115**, 084506 (2014); 10.1063/1.4866872

Thermoelectric performance of MX2 (M=Mo,W; X=S,Se) monolayers
J. Appl. Phys. **113**, 104304 (2013); 10.1063/1.4794363

Phonons in MS2 (M=Mo, W) Nanotubes
AIP Conf. Proc. **899**, 383 (2007); 10.1063/1.2733197

Resonance Raman scattering in bulk 2H-MX$_2$ (M = Mo, W; X = S, Se) and monolayer MoS$_2$

Jia-He Fan,[1] Po Gao,[1] An-Min Zhang,[1] Bai-Ren Zhu,[2] Hua-Ling Zeng,[2] Xiao-Dong Cui,[2] Rui He,[3] and Qing-Ming Zhang[1,a)]

[1]*Department of Physics, Renmin University of China, Beijing 100872, People's Republic of China*
[2]*Department of Physics, The University of Hong Kong, Pokfulam Road, Hong Kong, People's Republic of China*
[3]*Department of Physics, University of Northern Iowa, Cedar Falls, Iowa 50614, USA*

We have performed a comparative study of resonance Raman scattering in transition-metal dichalcogenides 2H-MX$_2$ semiconductors (M = Mo, W; X = S, Se) and single-layer MoS$_2$. Raman spectra were collected using excitation wavelengths 633 nm (1.96 eV), 594 nm (2.09 eV), 532 nm (2.33 eV), 514 nm (2.41 eV), and 488 nm (2.54 eV). In bulk-MoS$_2$ and WS$_2$, the resonant energies appear to coincide with their exciton excitations. The resonance can be fine tuned by varying sample temperatures, which confirms its excitonic origin in both MoS$_2$ and WS$_2$. Temperature dependence of Raman intensities is analyzed in the context of resonance Raman theory, which agrees well with the existing absorption data. While in WSe$_2$, the resonance has been observed in a wider range of excitations from 633 to 514 nm, which cannot be explained with its excitonic energies of 1.6 and 2.0 eV. It is considered that additional excitonic bands induced by band splitting are involved in the inter-band transitions and substantially extend the resonance energy range. The Raman resonance energy range remains unchanged in single-layer MoS$_2$ compared with that in the bulk sample. However, most phonon modes in single-layer MoS$_2$ are significantly broadened or strongly suppressed under resonance conditions. This change could be related to the modification of acoustic modes by the substrate. © 2014 AIP Publishing LLC.
[http://dx.doi.org/10.1063/1.4862859]

INTRODUCTION

The transition-metal dichalcogenides 2H-MX$_2$ semiconductors (M = Mo, W; X = S, Se) are layered compounds very similar to graphite. MX$_2$ layers are held together by weak van der Waals interaction, so atomically thin MX$_2$ flakes can be easily exfoliated from bulk crystal.[1] The similarity between the two layered systems has attracted extensive interests in the two-dimensional materials. Single-layer MX$_2$ exhibits many unique properties, for example, surprisingly high photoluminescence (PL) efficiency,[2,3] a clear spin splitting of valence bands due to strong spin-orbit coupling,[4–8] and a novel spin-valley coupling,[9–15] etc. In spite of its structural similarity to graphene, layered MX$_2$ has some advantages over graphene. Originally, it is a semiconductor and has intrinsic band-gaps. Furthermore, photoluminescence and absorption measurements reveal that the indirect band-gap in bulk crystal evolves into a direct one in single-layer MoS$_2$,[15–19] which is also predicted by theory.[20–23] These properties make MX$_2$ more flexible than graphene in electronic device applications.

Raman scattering is proved to be a key technique in both determining the number of layers and probing band excitations in few-layer MX$_2$ and graphene.[24–31] In a general Raman process, Raman intensities I_{ph} are proportional to scattering probability P_{ph} which is described by three-step time-dependent perturbation theory as following:[32–34]

$$I_{ph} \propto P_{ph} \propto \left| \frac{\langle f|H_{e-R}(\omega_s)|m'\rangle\langle m'|H_{e-p}|m\rangle\langle m|H_{e-R}(\omega_i)|i\rangle}{(E_{im} - \hbar\omega_i - i\Gamma_1)(E_{m'f} - \hbar\omega_s - i\Gamma_2)} \right|^2,$$ (1)

where $|i\rangle$, $|f\rangle$, and $|m\rangle/|m'\rangle$ are initial, final, and intermediate states, respectively; H_{e-R} and H_{e-p} the electron-radiation interaction and electron-phonon interaction Hamiltonians, respectively; E_{im} and $E_{m'f}$ the energy differences between initial and intermediate states and between final and intermediate states, respectively; ω_i and ω_s the incident and scattered photon frequencies, respectively. Γ_1 and Γ_2 are damping constants which are related to the lifetimes of the intermediate states. If intermediate states are real conduction/excitonic bands rather than virtual states, $E_{im}/E_{m'f}$ exactly measures band/excitonic excitation gaps. In this case, when $\hbar\omega_i$ or $\hbar\omega_s$ approaches gap energies, Raman scattering intensity will be enhanced dramatically as seen in Eq. (1). In fact, Eq. (1) provides a basis for quantitatively analyzing excitonic excitations and temperature dependence of phonon intensities in the vicinity of resonance. If the 1 s exciton state is well separated from other states and is the main intermediate state that contributes to Raman scattering in transition-metal dichalcogenide system we study, Eq. (1) can be simplified to[32–34]

$$I_{ph} \propto \left| \frac{1}{[E(T) - \hbar\omega_i - i\Gamma(T)] \times [E(T) - \hbar\omega_s - i\Gamma(T)]} \right|^2,$$ (1a)

a)qmzhang@ruc.edu.cn

where all the matrix elements are incorporated into a constant (not shown here), $E(T)$ and $\Gamma(T)$ are temperature-dependent transition energies and damping of exciton, which will be discussed in more detail later.

This resonance Raman scattering creates an important avenue to studies of band/excitonic excitations in diverse nanomaterials.[34–37] It also offers unique insight into multi-phonon process due to the relaxation of selection rules and a huge amplification of Raman intensity under the resonance condition. Fortunately, the direct gaps of all the above MX_2 bulk crystals and few-layer flakes ($\sim$1.5 eV–2.5 eV)[38] overlap the photon energies of visible light, which enables our studies of resonance Raman scattering in these materials by using visible laser excitations.

MX_2 (M = Mo, W; X = S, Se) compounds share the similar crystal structure and symmetry, where Raman-active modes E_{1g}, A_{1g}, $E_{2g}(1)$, and $E_{2g}(2)$ are arised.[39–45] There have been some reports of resonance Raman scattering in bulk MoS_2 and WS_2, in which multi-phonon modes composed of optical A_{1g}/E^1_{2g} and longitudinal acoustic (LA) phonons were clearly observed under the resonance conditions.[46–50] Livneh and Sterer carefully studied pressure and temperature-dependent Raman resonance in bulk $2H$-MoS_2 and pointed out that the excitonic excitations offer the resonance enhancement of Raman intensities. Despite the sporadic reports, comprehensive study of resonance Raman scattering in bulk $2H$-MX_2 and single-layer flake is still lacking.

In this paper, we report resonance Raman study of bulk $2H$-MoS_2, WS_2, WSe_2, and monolayer MoS_2. Resonance Raman spectra of MoS_2 and WS_2 can be well understood in terms of excitonic band excitations. This interpretation naturally explains why resonance Raman spectra show a systematic evolution with varying temperature which is equivalent to the fine tuning of excitonic band gaps. The resonance in WSe_2 remains at excitation energies even higher than its excitonic band gaps. It is believed that additional excitonic states induced by band splitting are involved in the resonance and effectively extend the energy range of resonance. This is also supported by the existing absorption spectra. We further measured Raman spectra of single-layer MoS_2 under several excitation wavelengths. The energy at which resonance occurs seems to be unchanged in comparison with that of bulk crystal. Interestingly, under the resonance condition, many observed modes, including multi-phonon ones, are significantly broadened and their intensities are weaker. This cannot be simply attributed to the change of electronic or phononic band structures with the transition from bulk to monolayer. The anomalous phonon change is considered to be affected by the acoustic modes in monolayer MoS_2, which participate in most of the observed multi-phonon processes but are modified by the interaction with substrates in the monolayer case.

EXPERIMENTAL PROCEDURES

Single-layer MoS_2 was obtained by exfoliation from bulk MoS_2 crystals (SPI Supplies) and placed on a Si wafer coated with 300 nm-thick oxide layer. Single layer MoS_2 can be identified under an optical microscope by color contrast.

Lateral size of single-layer MoS_2 is estimated to be $\sim$5 $\times$ 10 μm^2. The number of MoS_2 layers was confirmed by frequency separation between $E_{2g}(1)$ and A_{1g} modes (see the inset of Fig. 6). Bulk WS_2 and WSe_2 were prepared by chemical vapor deposition (CVD) method.[19] Raman spectra with five excitation wavelengths were measured using different spectrometers. We employed Jobin Yvon T64000 system for 633 nm (Melles Griot, HeNe Laser) and 532 nm (Torus 532, Laser Quantum) excitations, and PI TriVista system for 594 nm (Cobolt Mambo) and 488 nm (Coherent Sapphire) excitations. The spectra at 514 nm (Melles Griot, Argon Laser) were measured with WITec-Alpha micro-Raman system. A backscattering configuration was adopted in all the measurements. For 594 and 488 nm excitations, the cut-off wavenumbers of edge filters are $\sim$300 and 200 cm^{-1}, a little higher than the other three cases. Variable-temperature measurements were conducted in a Janis ST-500E cryostat under a vacuum of $\sim$10^{-7} mbar. Variable-temperature PL spectra were measured at 633 nm excitation using the T64000 system.

RESULTS AND DISCUSSIONS

Fig. 1 shows Raman spectra of bulk MoS_2 collected at different excitation wavelengths. Only two Raman-active modes E^1_{2g} and A_{1g} can be seen with 488 and 532 nm excitations. Many additional modes appear in the Raman spectra when 594 nm (2.09 eV) and 633 nm (1.96 eV) lasers are applied. The resonance at 633 nm has been studied by several groups,[46,47,51] which can be well understood as facilitated by excitonic excitations in the vicinity of A($\sim$1.88 eV) exciton. The additional modes were also assigned to multi-phonon lines. The 466 cm^{-1} mode with strong intensity is attributed to a combination of two LA modes. Similarly, the combinations between LA modes and E_{2g}, A_{1g} E_{1g}, E_{1u} optical modes can explain most of the additional lines at higher frequencies.[47] The resonance at 594 nm is similar to that occurs at 633 nm case, despite the small discrepancy in the relative intensities between different modes. Naturally one can associate the excitation energy with the energy of B exciton, which is about 2.06 eV at room
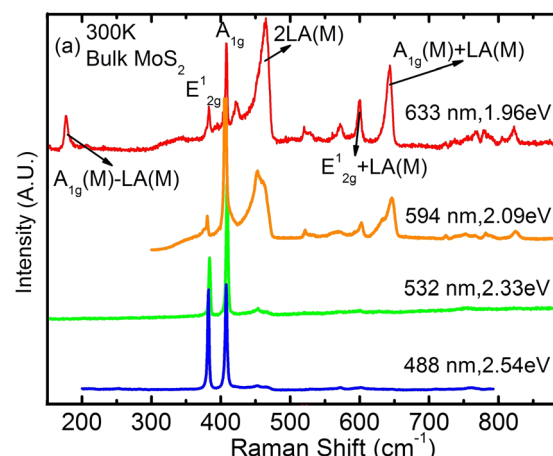

FIG. 1. Raman spectra of bulk MoS_2 crystal under different excitation wavelengths at room temperature.

temperature.[52] As revealed in our resonance Raman experiments, both the A and B excitons formed at K/K′ points are involved in the optical resonance processes. On the other hand, the excitonic gaps can be smoothly changed by external conditions like temperature or pressure.[51,53] This means that we can fine tune the excitonic gaps by varying temperature or pressure and hence the resonance condition to further confirm the resonance enhancement mechanism by monitoring the evolution of excitonic gaps with temperature or pressure.

Under non-resonant conditions, temperature dependence of Raman intensities is governed by the Bose-Einstein thermal factor. However, Raman resonance plays a more important role in Raman intensities compared with phonon thermal population. Fig. 2(a) shows Raman spectra of bulk 2H-MoS_2 collected at different temperatures under a 633 nm laser excitation. The spectra exhibit a continuous and rapid increase in intensity with decreasing temperature. For a qualitative view, the inset of Fig. 2(a) shows the temperature dependence of integrated spectral intensities from 135 to 1200 cm^{-1}, which demonstrates a nearly linear decrease in the integrated intensity with increasing temperature. And the integrated intensity at 70 K is almost nine times higher than that at 300 K. As a comparison, we also measured Raman spectra of the same sample at different temperatures using a 532 nm laser excitation, as depicted in Fig. 2(b). The dramatic changes in spectral intensities observed under a 633 nm laser excitation completely disappear. Clearly, it is out of resonance due to the relatively large difference between the excitation photon energy and the excitonic transition energies in the material.[51] With decreasing temperature, the gap of A exciton is fine tuned and approaches the

photon energy of 633 nm incident light,[54] which causes the rapid enhancement of Raman scattering intensities.

In order to obtain quantitative information from our resonance measurements, we plot the temperature dependence of integrated intensities of A_{1g} mode in Fig. 3(a). The formula (1a) can be used to fit the data when the functional forms of $E(T)$ and $\Gamma(T)$ are given. The temperature dependence of excitonic transition energies follows Varshini empirical relationship[51]

$$E(T) = E(0) - \frac{\alpha T^2}{(\beta + T)}, \tag{2}$$

where $E(0)$ and $E(T)$ are transition energies of exciton at 0 K and finite temperatures, and α and β are the fitting parameters related to exciton-phonon interaction and Debye temperature, respectively. The temperature dependence of exciton damping is given by[55]

$$\Gamma(T) = \Gamma_0 + \frac{\Gamma_{ph}}{\exp(\Theta_{ph}/T) - 1}, \tag{3}$$

where Γ_0 is the temperature-independent width, Γ_{ph} is the exciton-phonon coupling strength, and Θ_{ph} is the phonon temperature. Combining (1a) with (2) and (3), we have made a perfect fitting of the temperature dependent intensity of the A_{1g} mode (shown in Fig. 3(a)). The fitting quantitatively determines the evolution of excitonic transition energies and damping with temperature, which are shown in Fig. 3(b). The evolution is in excellent agreement with the results from absorption measurements.[55] Note that the damping of exciton, corresponding to full width at half maximum (FWHM), is adopted in our analysis.
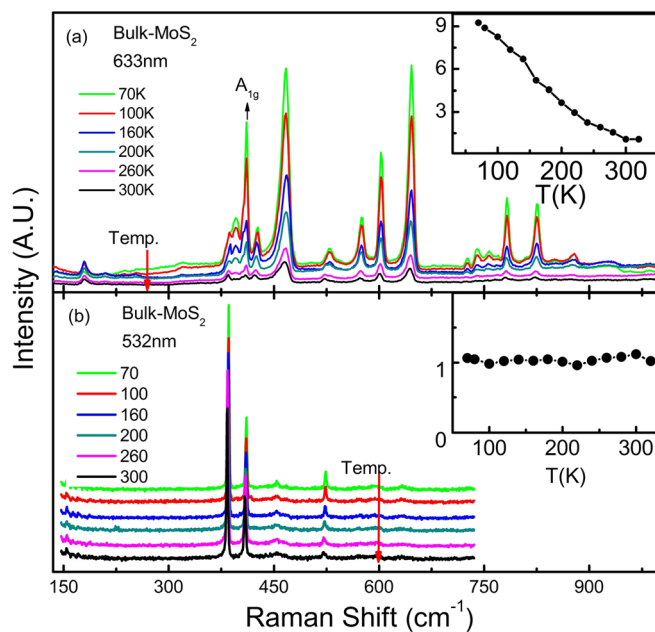

FIG. 2. Raman spectra of bulk 2H-MoS_2 at selected temperatures under 633 nm (a) and 532 nm (b) excitations, respectively. The integrated intensities have been corrected with Bose-Einstein thermal factor and normalized to the values at 320 K. To illustrate the resonance behaviors, the insets show the temperature dependence of normalized integrated intensity of Raman phonons in the energy range of 135–1200 cm^{-1} under 633 nm excitation and 135–700 cm^{-1} for 532 nm excitation.
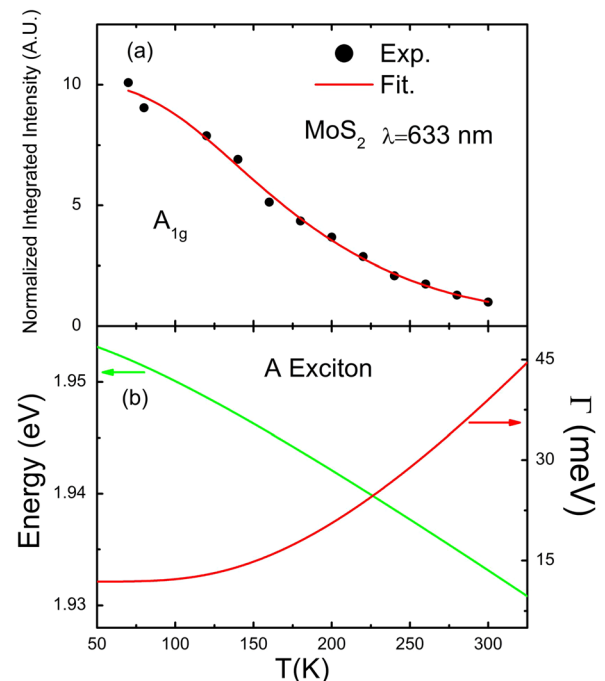
FIG. 3. (a) Normalized integrated intensities of A_{1g} mode versus temperature. The solid red line is the fitting curve using formula (1a) in combination with (2) and (3). The fitting determines the parameters as following: E(0) = 1.954 eV, α = 0.101 meV/K, β = 122 K, Γ_0 = 11.8 meV, Γ_{ph} = 193 meV, Θ_{ph} = 628 K. (b) Calculated temperature dependence of transition energies and damping of A exciton in MoS_2 using (2) and (3). Parameters are taken from the fitting in (a).

In addition to absorption experiment, PL spectroscopy is another widely used technique to study the resonance. Unfortunately, PL signal is very weak in bulk MoS_2 because it is an indirect-gap semiconductor. However, in mononlayer MoS_2, the excitonic transition gap at K points in the Brillouin zone evolves into a direct gap and PL signal is dramatically enhanced by more than three orders of magnitude.[16–18] It means that alternatively, one can see the excitonic process through the enhanced PL spectra in the monolayer case. Fig. 4 shows PL spectra of monolayer MoS_2 at selected temperatures. The well-defined PL peak in Fig. 4(a), whose position defines the transition energy of A exciton, smoothly shifts towards low energy and its width becomes broader when temperature increases. We also fit the peak positions versus temperature using Eq. (2). The temperature evolution is well consistent with that of near-resonance Raman spectra discussed above.

Fig. 5 gives Raman spectra of WS_2 under five excitation wavelengths. Raman-active E_{2g}^1 and A_{1g} modes exist in all the five spectra. Additional modes can be observed in all the spectra except the one excited by a 488 nm laser excitation. It indicates that Raman resonance in WS_2 covers a large energy range from 1.96 to 2.41 eV. The excitonic gaps for A and B excitons are 1.95 and 2.36 eV at room temperature,[52] respectively. It provides an initial understanding for the large resonance range. We can assign the resonance at 633 nm (1.96 eV) to A exciton,[54] and those at 532 nm (2.33 eV) and 514 nm (2.41 eV) to B exciton due to its broad features revealed by absorption experiments.[56] The resonance at 594 nm (2.09 eV) is unusual. It may be assisted by intermediate process, like higher-order excitonic states. A completely reliable interpretation will depend on a detailed knowledge of the electronic band structures. A comprehensive and self-consistent understanding of such a large resonance energy range is an open question raised by the present resonance Raman experiments in WS_2.

Fig. 6(a) shows resonance Raman spectra of bulk 2H-WS_2 using a 633 nm laser light at various temperatures. The

FIG. 5. (a) Raman spectra of bulk 2H-WS_2 at five excitation wavelengths. (b) Same spectra as in (a) with magnified intensities for a clearer view of weak features.
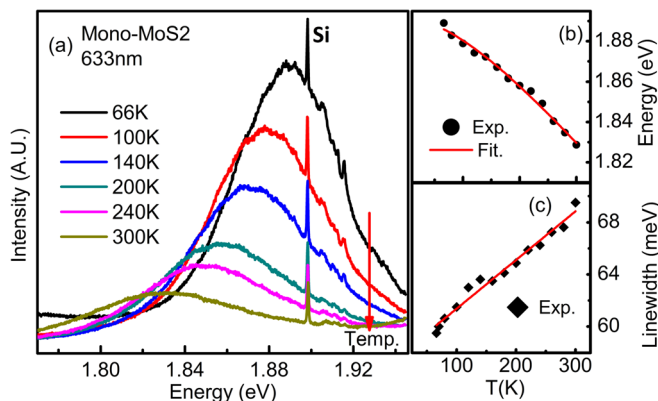

FIG. 4. (a) Photoluminescence spectra of monolayer MoS_2 at selected temperatures under 633 nm excitation. The sharp peak superimposed on the PL peak, is the phonon line from substrate Si. (b) Temperature dependence of PL peak positions drawn from (a). The solid red line is the fitting curves following Eq. (2). The fitting parameters are $E(0) = 1.891$ eV, $\alpha = 0.371$ meV/K, $\beta = 243$ K. (c) Temperature dependence of PL peak widths. The red line is a guide to the eye.
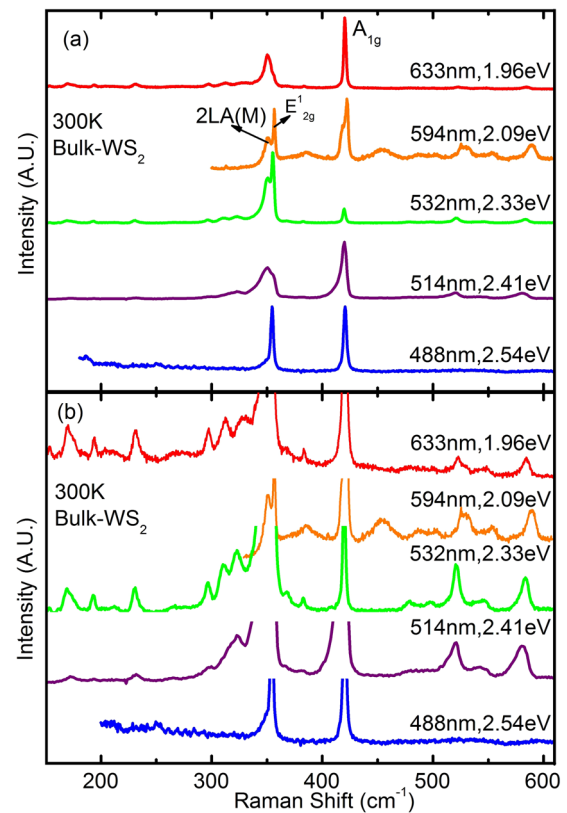
resonance becomes much stronger with increasing temperature. The background at low wavenumbers in Fig. 6(a) continuously rises with increasing temperatures, which is attributed to the photoluminescence of A exciton. Intensity enhancement with temperature is also found for most of the modes in the spectra excited by a 532 nm laser light (Fig. 6(b)). For the 2LA(M) mode at 350 cm^{-1} (shown in the inset of Fig. 6(b)), the intensity increases and the frequency displays a redshift with increasing temperature. Similar to the case of MoS_2, the temperature evolutions reflect the fine-tuning of A and B excitonic gaps. It should be noted that the spectral evolutions with temperatures in both 633 and 532 nm cases are opposite to that of MoS_2 mentioned above. In MoS_2, excitonic transition energies are at 1.88 (A) and 2.06 (B) eV at room temperature. As temperature decreases, the energy of the A exciton gradually approaches the photon energy of the laser light (633 nm) and hence Raman intensity rapidly increases. Whereas in WS_2, the A and B exciton energies are at 1.96 eV (close to the photon energy of 633 nm) and 2.33 eV (close to the photon energy of 532 nm) at room temperature. As temperature decreases, both excitonic energies increase and are away from the photon energies. Therefore, Raman scattering intensities continuously decrease with lowered temperature. In other words, the fine-tuning by temperature has different effects on MoS_2 and WS_2, i.e., close to and away from the resonance, respectively. Figs. 7(a) and 7(c) quantitatively present the integrated intensities of the A_{1g} phonon versus excitonic transition energies for A and B excitons, respectively. Just
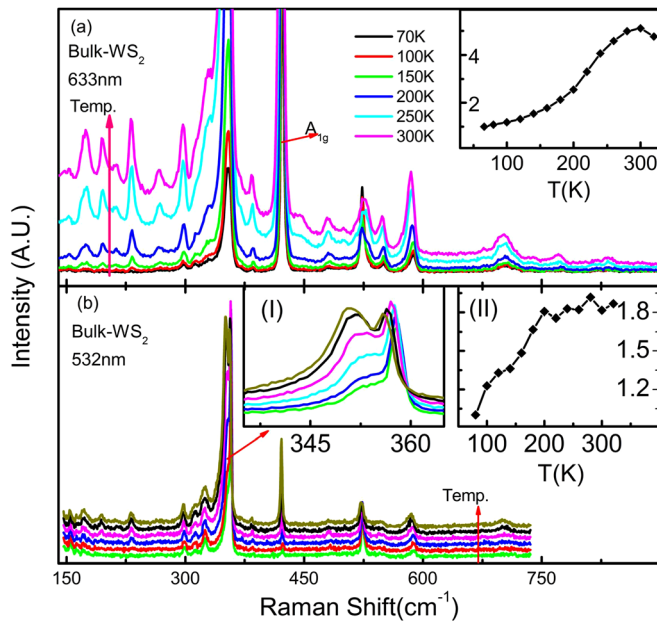
FIG. 6. Raman spectra of bulk 2H-WS$_2$ at selected temperatures under 633 (a) and 532 nm (b) excitations. For a qualitative view, the inset in (a) and the right inset in (b) show the temperature dependence of integrated intensities in the same way as we show in Fig. 2. The left inset in (b) shows temperature evolution of 2LA(M) and E$_{2g}^1$ modes around 350 cm^{-1}.

like the MoS$_2$ case, the expression (1a) can also be applied here to produce perfect fittings (solid red lines in Figs. 7(a) and 7(c)). This indicates that the fine-tunable Raman enhancement in WS$_2$ can be well understood in term of excitonic resonance. This is also supported by absorption spectra in WS$_2$.[55] Furthermore, the information on transition energies and damping of A and B excitons can be drawn from the fittings, as we have seen in MoS$_2$. Figs. 7(b) and 7(d) demonstrate their temperature evolutions, which are calculated based on formula (2) and (3) with the parameters determined by the fittings in Figs. 7(a) and 7(c). The results also quantitatively overlap with those obtained from absorption experiments.[55]
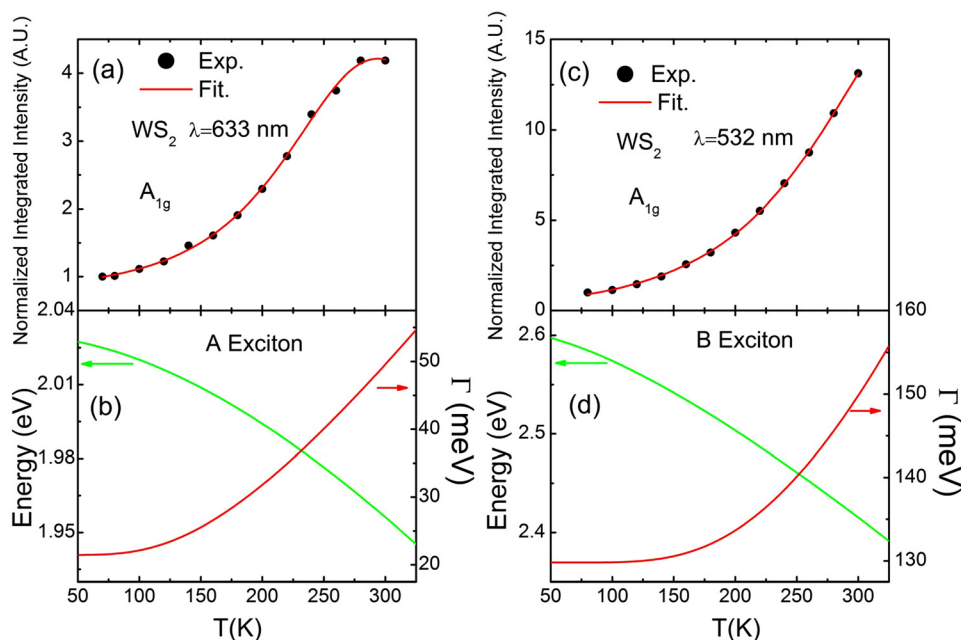
Fig. 8 shows Raman spectra of bulk WSe$_2$ at different excitations. It should be noted that only a sharp mode located at 250 cm^{-1} is observed in the spectrum with 488 nm excitation. It has been reported that this mode actually consists of nearly degenerate E$_{2g}^1$ and A$_{1g}$ modes.[24,42] While for the other four excitations, many additional modes are seen and they appear to be quite similar under different excitations. Just like the case of WS$_2$, the resonance also covers a wide energy range at least from 1.96 to 2.41 eV. However, the measured gaps of A and B excitons in WSe$_2$ are at about 1.65 and 2.0 eV, respectively,[4,38] which are much lower than the energy range in which resonance occurs. Therefore, Raman resonance in WSe$_2$ cannot be simply explained as the excitonic excitations. It was pointed out that different from sulfur ions in MoS$_2$ and WS$_2$, Se has a larger ionic radius and hence a larger overlap between Se orbitals from adjacent layers.[38] This would induce a band splitting and bring additional excitonic bands. In fact, absorption measurements observed not only the peaks contributed by A and B excitons, but also the ones originated from A$'$ and B$'$ excitons which were considered to be caused by band splitting.[4,38] Then the resonance at 633 nm (1.96 eV) and 594 nm (2.09 eV) can be assigned to B exciton and the ones at 532 nm (2.33 eV) and 514 nm (2.41 eV) to A$'$ exciton.

In Figs. 1, 5, 8, and 9, abundant higher-order phonon processes can be clearly seen under resonance conditions in the bulk and monolayer samples. Some of them in MoS$_2$ and WS$_2$ have been assigned in Refs. 46 and 47, while a comprehensive assignment of the multi-phonons in WSe$_2$ is still lacking. It requires complicated LDA calculations of joint density of states for multi-phonon processes and a careful symmetry analysis under conservations of energy and momentum, which is apparently beyond the scope of the present paper. Nevertheless, the clear regular phonon bands seen in Fig. 8 offer insight on multi-phonons in WSe$_2$. The "period" of phonon bands is about 250 cm^{-1}, which may be an indication of the LA(M) acoustic mode as in MoS$_2$ and WS$_2$.

FIG. 7. Normalized integrated intensities of A$_{1g}$ mode versus temperature with 633 nm (a) and 532 nm (c) excitations. The solid red lines in (a) and (c) are the fitting curves using formula (1a) in combination with (2) and (3). The fittings give the parameters E(0) = 2.038 eV, α = 0.949 meV/K, β = 858 K, Γ(0) = 21.5 meV, Γ_{ph} = 137 meV, Θ_{ph} = 532 K for A exciton; E(0) = 2.607 eV, α = 1.210 meV/K, β = 268 K, Γ_0 = 130 meV, Γ_{ph} = 488 meV, Θ_{ph} = 969 K for B exciton. Calculated temperature dependence of transition energies and damping of A exciton (b) and B exciton (d) in WS$_2$ using (2) and (3). Parameters are taken from the fittings in (a) & (c).
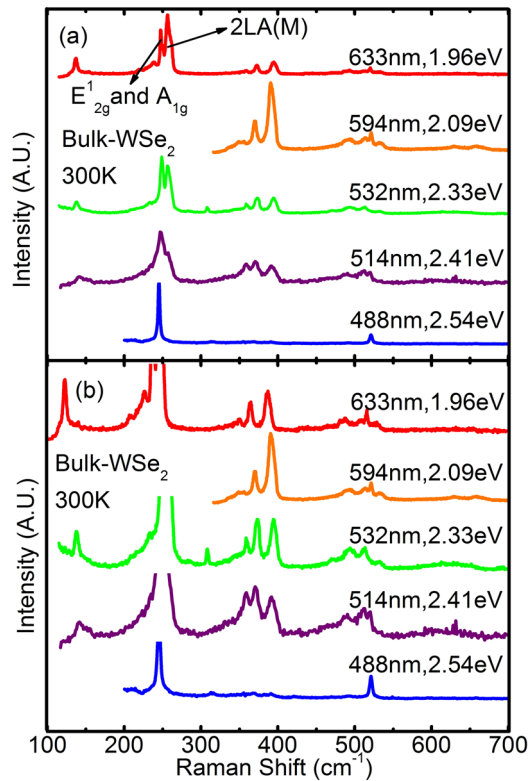
FIG. 8. (a) Raman spectra of bulk WSe$_2$ at five excitation wavelengths. (b) Same spectra as in (a) with magnified intensities.

Resonance Raman scattering in single-layer MoS$_2$ is shown in Fig. 9. Just like in the bulk, the resonance still occurs at 633 nm (1.96 eV) and 594 nm (2.09 eV). It seems that the resonance energy range is almost unaffected by the transition from indirect to direct gap when reducing bulk MoS$_2$ to one layer. It suggests that the resonance is always dominated by the excitonic excitations at K/K' in both bulk and single-layer MoS$_2$. One difference between the resonance spectra of the bulk and single-layer is the gradual lift-up of background towards high frequencies in monolayer MoS$_2$. Clearly it comes from the tail of extremely strong photoluminescence in monolayer MoS$_2$. A significant
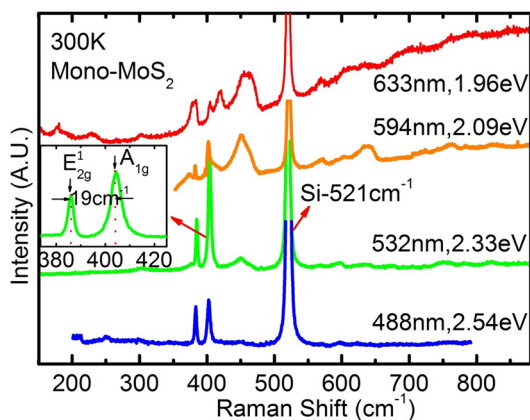

FIG. 9. Room-temperature Raman spectra of monolayer MoS$_2$ under different excitation wavelengths. The inset shows the frequency separation between E$_{2g}^1$ and A$_{1g}$ modes, which demonstrates that the sample is a monolayer MoS$_2$.

difference between bulk and monolayer MoS$_2$ in resonance Raman spectra is that almost all the first-order and multi-phonon modes are greatly broadened and their relative intensities are substantially changed in the monolayer MoS$_2$. The sharp multi-phonon modes above 550 cm^{-1} in the resonance spectra of the bulk are strongly suppressed and almost invisible in the monolayer case. It seems that sample quality is not the answer to the question because E$_{2g}^1$ and A$_{1g}$ modes remain very sharp under the non-resonance condition in monolayer MoS$_2$. Similar results were also reported in a recent Raman paper.[57]

There are several possible reasons for the suppression of Raman modes above 550 cm^{-1} in monolayer MoS$_2$. One reason could be the change of electronic band structures with the transition from bulk to monolayer. As we mentioned earlier, the resonance originates from the excitonic excitations at K/K' and is not sensitive to the subtle changes of band structures in other k-points. In this scenario, the change of electronic band structures may be just a minor factor causing the suppression. Another possibility could be the change of phonon band structures. It seems that this may provide a direct explanation for the phonon anomaly in monolayer. However, first-principles calculations indicate that phonon dispersion only has a negligible discrepancy between bulk and monolayer MoS$_2$.[39] The third possibility is that the acoustic branches in monolayer are strongly affected by substrate. In bulk case, the first layer in contact with the substrate only consists of a tiny amount of atoms in the whole sample and has little impact on the lattice vibrations. However, in the monolayer, the situation is completely changed. The long-range acoustic modes are easily affected by additional forces provided by the substrate. Under the resonance conditions, the acoustic modes are involved in most of the observed additional modes. In other words, the modification of acoustic modes by the substrate causes the suppression of most multi-phonon process.

SUMMARY

In summary, we conducted a comparative resonance Raman scattering study on bulk 2H-MX$_2$ semiconductors (M = Mo, W; X = S, Se) and single-layer MoS$_2$. We found that Raman resonance can be conveniently understood with the excitonic excitations at K/K' in bulk MoS$_2$. In bulk WS$_2$, beyond A and B first-order excitonic states involved in the resonance, some other intermediate process like higher-order excitonic states, are needed to explain the resonance at 594 nm (2.09 eV), which is slightly away from A excitonic energies. The resonance is fine tuned by varying temperatures in MoS$_2$ and WS$_2$, which is consistent with the excitonic picture. However, in WSe$_2$, it is impossible to understand the wide resonance energy range in terms of the first-order energies of A and B excitons. The wide energy range of resonance in WSe$_2$ can be understood by considering the additional exciton states. The present resonance Raman experiments reveal a general trend that 5d elements in 2H-MX$_2$ bring more complicated band features than 4d elements. It raises some important issues on fine band structures in 2H-MX$_2$ compounds. Raman resonance in

single-layer MoS_2 is similar to the bulk to some extent. But most of the first-order and multi-phonon modes in monolayer are greatly broadened or suppressed. We interpret the anomalous phonon change in terms of the modified acoustic modes by the substrate. It suggests that one needs to take into account the impact of the substrate when exploring the physical properties of monolayer MoS_2.

ACKNOWLEDGMENTS

[1]K. S. Novoselov, D. Jiang, F. Schedin, T. J. Booth, V. V. Khotkevich, S. V. Morozov, and A. K. Geim, Proc. Natl. Acad. Sci. U.S.A. **102**, 10451 (2005).

[2]A. Splendiani, L. Sun, Y. B. Zhang, T. S. Li, J. Kim, C. Y. Chim, G. Galli, and F. Wang, Nano Lett. **10**, 1271 (2010).

[3]R. S. Sundaram, M. Engel, A. Lombardo, R. Krupke, A. C. Ferrari, Ph. Avouris, and M. Steiner, Nano Lett. **13**, 1416 (2013).

[4]R. A. Bromleyt, R. B. Murray, and A. D. Yoffe, J. Phys. C: Solid State Phys. **5**, 759 (1972).

[5]E. S. Kadantsev and P. Hawrylak, Solid State Commun. **152**, 909 (2012).

[6]A. Ramasubramaniam, Phys. Rev. B **86**, 115409 (2012).

[7]R. Coehoorn and C. Haas, Phys. Rev. B **35**, 6203 (1987).

[8]Z. Y. Zhu, Y. C. Cheng, and U. Schwingenschlög, Phys. Rev. B **84**, 153402 (2011).

[9]H. L. Zeng, J. f. Dai, W. Yao, D. Xiao, and X. D. Cui, Nat. Nanotechnol. **7**, 490 (2012).

[10]T. Cao, G. Wang, W. P. Han, H. Q. Ye, C. R. Zhu, J. R. Shi, Q. Niu, P. H. Tan, E. Wang, B. L. Liu, and J. Feng, Nat. Commun. **3**, 1882 (2012).

[11]G. Sallen, L. Bouet, X. Marie, G. Wang, C. R. Zhu, W. P. Han, Y. Lu, P. H. Tan, T. Amand, B. L. Liu, and B. Urbaszek, Phys. Rev. B **86**, 081301(R) (2012).

[12]K. F. Mak, K. L. He, J. Shan, and T. F. Heinz, Nat. Nanotechnol. **7**, 494 (2012).

[13]A. M. Jones, H. Yu, N. J. Ghimire, S. Wu, G. Aivazian, J. S. Ross, B. Zhao, J. Yan, D. G. Mandrus, D. Xiao, W. Yao, and X. Xu, e-print arXiv:1303.5318 (2013).

[14]X. D. Xu, D. Xiao, and W. Yao, SPIE Proc. **86**, 35 (2013).

[15]D. Xiao, G. B. Liu, W. X. Feng, X. D. Xu, and W. Yao, Phys. Rev. Lett. **108**, 196802 (2012).

[16]K. F. Mak, C. Lee, J. Hone, J. Shan, and T. F. Heinz, Phys. Rev. Lett. **105**, 136805 (2010).

[17]W. J. Zhao, Z. Ghorannevis, L. Q. Chu, M. L. Toh, C. Kloc, P. H. Tan, and G. Eda, ACS Nano **7**, 791–797 (2013).

[18]S. Tongay, J. Zhou, C. Ataca, K. Lo, T. S. Matthews, J. B. Li, J. C. Grossman, and J. Q. Wu, Nano Lett. **12**, 5576 (2012).

[19]H. L. Zeng, G. B. Liu, J. F. Dai, Y. J. Yan, B. R. Zhu, R. C. He, L. Xie, S. J. Xu, X. H. Chen, W. Yao, and X. D. Cui, Sci. Rep. **3**, 1608 (2013).

[20]S. W. Han, H. Kwon, S. K. Kim, S. Ryu, W. S. Yun, D. H. Kim, J. H. Hwang, J. S. Kang, J. Baik, H. J. Shin, and S. C. Hong, Phys. Rev. B **84**, 045409 (2011).

[21]Y. C. Cheng, Z. Y. Zhu, and U. Schwingenschlög, RSC Adv. **10**, 1039 (2012).

[22]W. S. Yun, S. W. Han, S. C. Hong, I. G. Kim, and J. D. Lee, Phys. Rev. B **85**, 033305 (2012).

[23]A. Kuc, N. Zibouche, and T. Heine, Phys. Rev. B **83**, 245213 (2011).

[24]W. J. Zhao, Z. Ghorannevisa, A. K. Kumar, J. R. Pang, M. L. Tohd, X. Zhang, C. Klocd, P. H. Tan, and G. Eda, arXiv:1204.0911 (2013).

[25]S. L. Li, H. Miyazaki, H. S. Song, H. Kuramochi, S. Nakaharai, and K. Tsukagoshi, ACS Nano **6**(8), 7381 (2012).

[26]G. Plechinger, S. Heydrich, J. Eroms, D. Weiss, C. Schüller, and T. Korn, Appl. Phys. Lett. **101**, 101906 (2012).

[27]H. Li, Q. Zhang, C. C. R. Yap, B. K. Tay, T. H. T. Edwin, A. Olivier, and D. Baillargeat, Adv. Funct. Mater. **22**, 1385 (2012).

[28]X. Zhang, W. P. Han, J. B. Wu, S. Milana, Y. Lu, Q. Q. Li, A. C. Ferrari, and P. H. Tan, Phys. Rev. B **87**, 115413 (2013).

[29]C. Lee, H. Yan, L. E. Brus, T. F. Heinz, J. Hone, and S. Ryu, ACS Nano **4**, 2695 (2010).

[30]H. L. Zeng, B. R. Zhu, K. Liu, J. H. Fan, X. D. Cui, and Q. M. Zhang, Phys. Rev. B **86**, 241301(R) (2012).

[31]A. C. Ferrari, J. C. Meyer, V. Scardaci, C. Casiraghi, M. Lazzeri, F. Mauri, S. Piscanec, D. Jiang, K. S. Novoselov, S. Roth, and A. K. Geim, Phys. Rev. Lett. **97**, 187401 (2006).

[32]P. Yu and M. Cardona, *Fundamentals of Semiconductors* (Springer-Verlag, Berlin, 1999); R. Loudon, Proc. R. Soc. London, Ser. A **275**, 218 (1963).

[33]W. Hayes and R. Loudon, *Scattering of Light by Crystals* (John 540 Wiley & Sons, New York, 1978).

[34]J. E. Zucker, A. Pinczuk, D. S. Chemla, A. Gossard, and W. Wiegmann, Phys. Rev. Lett. **51**, 1293 (1983).

[35]R. He, I. Dujovne, L. W. Chen, Q. Miao, C. F. Hirjibehedin, A. Pinczuk, C. Nuckolls, C. Kloc, and A. Ron, Appl. Phys. Lett. **84**, 987 (2004).

[36]R. He, N. G. Tassi, G. B. Blanchet, and A. Pinczuk, Phys. Rev. B **83**, 115452 (2011).

[37]E. S. Freitas Neto, S. W. da Silva, P. C. Morais, M. I. Vasilevskiy, M. A. Pereira-da-Silva, and N. O. Dantas, J. Raman Spectrosc. **42**, 1660 (2011).

[38]A. R. Beal, J. C. Knights, and W. Y. Liang, J. Phys. C: Solid State Phys. **5**, 3540 (1972).

[39]A. M. Sánchez and L. Wirtz, Phys. Rev. B **84**, 155413 (2011).

[40]T. J. Wieting and J. L. Verble, Phys. Rev. B **3**, 4286 (1971).

[41]T. Sekine, M. Izumi, T. Nakashizu, K. Uchinokura, and E. Matsuura, J. Phys. Soc. Jpn. **49**, 1069 (1980).

[42]D. G. Mead and J. C. Irwi, Can. J. Phys. **55**, 379 (1977).

[43]J. L. Verble and T. J. Wieting, Phys. Rev. Lett. **25**, 362 (1970).

[44]S. Uchida and S. Tanakn, J. Phys. Soc. Jpn. **45**, 153 (1978).

[45]S. Jiménez Sandoval, D. Yang, R. F. Frindt, and J. C. Irwin, Phys. Rev. B **44**, 3955 (1991).

[46]G. L. Frey and R. Tenne, Phys. Rev. B **60**, 2883 (1999).

[47]B. C. Windom, W. G. Sawyer, and D. W. Hahn, Tribol. Lett. **42**, 301 (2011).

[48]T. Sekine, K. Uchinokura, T. Nakashizu, E. Matsuura, and R. Yoshizaki, J. Phys. Soc. Jpn. **53**, 811–818 (1984).

[49]M. Staiger, P. Rafailov, K. Gartsman, H. Telg, M. Krause, G. Radovsky, A. Zak, and C. Thomsen, Phys. Rev. B **86**, 165423 (2012).

[50]A. Berkdemir, H. R. Gutiérrez, A. R. Botello-Méndez, N. Perea-López, A. L. Elías, C. I. Chi, B. Wang, V. H. Crespi, F. López-Urías, J. C. Charlier, H. Terrones, and M. Terrones, Sci. Rep. **3**, 1755 (2013).

[51]T. Livneh and E. Sterer, Phys. Rev. B **81**, 195209 (2010).

[52]J. V. Acrivos, W. Y. Liang, J. A. Wilson, and A. D. Yoffe, J. Phys. C **4**, L18 (1971).

[53]T. Korn, S. Heydrich, M. Hirmer, J. Schmutzler, and C. Schuller, Appl. Phys. Lett. **99**, 102109 (2011).

[54]G. L. Frey and R. Tenne, J. Mater. Res. **13**, 2412 (1998).

[55]C. H. Ho, C. S. Wu, Y. S. Huang, P. C. Liao, and K. K. Tiong, J. Phys.: Condens. Matter **10**, 9317 (1998).

[56]J. R. Lince and S. V. Didziulis, Phys. Rev. B **43**, 4641 (1991).

[57]B. Chakraborty, H. S. S. Ramakrishna Matte, A. K. Sooda, and C. N. R. Rao, J. Raman Spectrosc. **44**, 4147 (2012).